Development/Plasticity/Repair

The Conserved Ig Superfamily Member Turtle Mediates Axonal Tiling in *Drosophila*

Kerry Ferguson, Hong Long, Scott Cameron, Wen-Tzu Chang, and Yong Rao

McGill Centre for Research in Neuroscience, and Department of Neurology and Neurosurgery, McGill University Health Centre, Montreal, Quebec H3G 1A4, Canada

Restriction of adjacent same-type axons/dendrites to separate single columns for specific neuronal connections is commonly observed in vertebrates and invertebrates, and is necessary for proper processing of sensory information. Columnar restriction is conceptually similar to tiling, a phenomenon referring to the avoidance of neurites from adjacent same-type neurons. The molecular mechanism underlying the establishment of columnar restriction or axonal/dendritic tiling remains largely undefined. Here, we identify Turtle (Tutl), a member of the conserved Tutl/Dasm1/IgSF9 subfamily of the Ig superfamily, as a key player in regulating the tiling pattern of R7 photoreceptor terminals in *Drosophila*. Tutl functions to prevent fusion between two adjacent R7 terminals, and acts in parallel to the Activin pathway. Tutl mediates homophilic cell–cell interactions. We propose that extrinsic terminal–terminal recognition mediated by Tutl, acts in concert with intrinsic Activin-dependent control of terminal growth, to restrict the connection made by each R7 axon to a single column.

Introduction

The phenomenon of columnar restriction in the nervous system is commonly observed in both vertebrates and invertebrates (Meinertzhagen and Hanson, 1993; Mountcastle, 1997). Columnar restriction is conceptually similar to axonal/dendritic tiling referring to the complete but non-overlapping coverage of the receptive fields by axons/dendrites from certain functionally homologous neurons (Wässle et al., 1981; Kramer and Kuwada, 1983). The establishment of tiling pattern involves both repulsion between same-type neurites (Wässle et al., 1981; Perry and Linden, 1982; Kramer and Kuwada, 1983; Grueber et al., 2003) and the intrinsic control of neurite growth (Lin et al., 2004; Ting et al., 2007). Recent studies identify Dscam as a repulsive tiling receptor in a small subset of neurons in *Drosophila* and mice (Millard et al., 2007; Fuerst et al., 2008). The identity of other cell surface proteins for tiling different neuronal cell types in the complex nervous system, however, remains unknown.

The *Drosophila* Tutl protein belongs to a novel and evolutionarily conserved subfamily of the Ig superfamily (see Fig. 1*A*). Previous studies show that Tutl and its mammalian homologs (i.e. Dasm1 in mice and IgSF9 in humans) are predominantly expressed in the nervous system (Bodily et al., 2001; Doudney et al., 2002; Shi et al., 2004a). Loss of *tutl* affects the larval locomotion behavior (Bodily et al., 2001). While previous *in vitro* studies suggest a role for Dasm1 in dendritic growth and synaptic development in cultured hippocampal neurons (Shi et al., 2004a,b), a recent *in vivo* study argues that lack of Dasm1 is not the cause of the previously observed dendrite phenotype (Mishra et al., 2008). Thus, the action of the Tutl/Dasm1/IgSF9 family proteins in the developing nervous system remains unclear.

We initiated our study on *tutl* due to its genetic interaction with *misshapen* (W. Ruan and Y. Rao, unpublished data), a known regulator of photoreceptor growth-cone motility in the *Drosophila* visual system (Ruan et al., 1999). The *Drosophila* visual system consists of the compound eye and the optic lobe. There are ~800 ommatidia in the compound eye, each containing eight different photoreceptor neurons (R cells), R1-R8. R1-R6 axons project into the first optic ganglion, the lamina, whereas R7 and R8 innervate the deeper medulla layer. Each R7 and R8 within the same ommatidium "see" the same point in space and terminate in a topographic manner in two layers within the same column, which also includes the axons of lamina neurons L1–L5 that relay the visual input from R1–R6 (Clandinin and Zipursky, 2002). Dscam2 is required for tiling L1 axons (Millard et al., 2007). Tiling of R7 terminals requires the Activin-mediated intrinsic growth control and mutual repulsion mediated by an unknown mechanism (Ting et al., 2007).

In this study, we determine the cellular function of Tutl in the *Drosophila* visual system. Our results show that Tutl controls R7 tiling by preventing fusion between adjacent R7 axons. We also show that Tutl mediates homophilic cell–cell interactions in cultured cells. Genetic analysis suggests that the Tutl-mediated terminal–terminal recognition functions in parallel to the intrinsic growth control mediated by the Activin pathway in R7 axonal tiling.

Received May 28, 2009; revised Sept. 10, 2009; accepted Sept. 14, 2009.

This work was supported by a Canadian Institutes of Health Research (CIHR) operating grant (MOP-14688) and a CIHR team grant (FRN#82501) awarded to Yong Rao, a CIHR postdoctoral fellowship to Kerry Ferguson, and a McGill University Health Centre studentship to Hong Long. Yong Rao is a Le Fonds de la Recherche en Santé de Québec senior research scholar. We thank members of the Rao laboratory and Donald van Meyel laboratory for comments and discussions; the Bloomington Stock Center and the Exelixis collection at Harvard Medical School for *tutl* mutant lines; Dr. Chi-Hon Lee for fly stocks and DNA reagents; Dr. Tzumin Lee for UAS-HLdActivin-RNAi line; Dr. Iris Salecker for *ey* $^{3.5}$-Flp and ELF fly stocks; and the *Drosophila* Genomic Resource Center (DGRC) for the RE40452 cDNA clone.

Correspondence should be addressed to Yong Rao, Centre for Research in Neuroscience, McGill University Health Centre, Room L7-136, 1650 Cedar Avenue, Montreal, QC H3G 1A4, Canada. E-mail: yong.rao@mcgill.ca.

DOI:10.1523/JNEUROSCI.2497-09.2009

 0270-6474/09/2914151-09$15.00/0

Materials and Methods

Genetics. *tutl*^{01085} and *tutl*^{K14703} were obtained from the Bloomington *Drosophila* Stock Center. Large clones (>90% of retina) of *tutl*^{01085} were generated in an otherwise heterozygous or wild-type eye by eye-specific mitotic recombination using the *ey*Flp/*FRT* system (Newsome et al., 2000). To visualize R7 and R8 axons in the eye-specific mosaic flies, genetic crosses were performed to generate *ey*Flp/+; *tutl*^{01085}, FRT40A/FRT40A, l(2); PanR7-GAL4, UAS-SynbGFP/+ and eyFlp/+; *tutl*^{01085}, FRT40A/FRT40A, [W+], l(2); Rh5/Rh6-GAL4, UAS-SynbGFP/+ progeny, respectively. To generate single mutant R7 axons with the MARCM system (Lee and Luo, 1999), flies were crossed to produce the following progeny: (1) *hs*Flp/+; *tutl*^{01085}, FRT40A/tub-GAL80, FRT40A; PanR7-GAL4, UAS-Synb-GFP/+ (flies were heat-shocked at 38°C for 1 h to induce mitotic recombination and were kept at 18°C to reduce background in wild-type cells); (2) GMR-Flp/+; *tutl*^{01085}, FRT40A/tub-GAL80, FRT40A; longGMR-GAL4, UAS-mCD8-GFP/+; and (3) *ey*$^{3.5}$-Flp/+; *tutl*^{01085}, FRT40A/tub-GAL80, FRT40A; longGMR-GAL4, UAS-mCD8-GFP/+. To examine loss of *tutl* specifically in the target region, we used the ELF (ey-Gal80, lama-Ga14, UAS-FLP) system (Chotard et al., 2005) to generate *ey*$^{3.5}$GAL80/+; *tutl*^{01085}, FRT40A/ubiGFP, cycE, FRT40A; lamaGAL4-UAS-Flp/+ progeny. *tutl*^{GAL4} was generated by jumping the GAL4 transgene on the C155 chromosome (X) to replace the P element in the *tutl*^{01085} allele on the second chromosome using the P-element replacement method described previously (Sepp and Auld, 1999). pBac[WH]*tutl*[f03096] and pBac[WH]*tutl*[f02770] were used to generate the deletion in *tutl*^{23} by using the FLP/FRT-based strategy described previously (Parks et al., 2004). For transgene rescue, genetic crosses were performed to generate the progeny: *tutl*^{K14703}/*tutl*^{23}; longGMR-GAL4/UAS-*tutl*. Transgenic RNAi experiments were performed by placing UAS-*tutl*-RNAi or UAS-HLdActivin RNAi under control of *tutl*-GAL4 or GMR-GAL4. To determine the potential genetic interaction between *tutl* and *imp-α3*, we crossed flies to generate the following progeny: GMR-Flp/+; *tutl*^{01085}, FRT40A/actinGAL4, UAS-mCD8-GFP; FRT82, *imp-α3*$^{17-76}$/FRT82, tub-GAL80 and GMR-Flp/+; +/actinGAL4, UAS-mCD8-GFP; FRT82, *imp-α3*$^{17-76}$/FRT82, tub-GAL80. Statistical analysis was performed using Student's *t* test. To examine whether elimination of neighboring R7 axons adjacent to *tutl* mutant R7 axons would affect column invasion, we used a temperature sensitive *sevenless* (*sev*) allele *sev*^{V1}. The MARCM system was used to generate and positively label homozygous *tutl* mutant R7 in hemizygous *sev*^{V1} males. At nonpermissive temperature (i.e., 25°C), the majority of R7 cells were eliminated, thus allowing us to examine the projection of isolated *sev*−R7 "escaper" cells that were also homozygous for the *tutl* mutation.

Molecular biology. To generate the *tutl*-RNAi transgene, two primers 5′ CCT *GAA TTC* ATG GGC GTG TGC GCG G 3′ and 5′ GTC *TCT AGA* CGC TAG AAG GGC CAG C 3′ were used to amplify ~400 bp sequence encoding the N-terminal 123 amino-acid sequence by PCR. Inverted repeats by self-ligation of the PCR fragments were subcloned into pMF3, which is a modified pUAST vector containing 10 GAL4-responsive UAS elements, similar to that described previously (Dietzl et al., 2007). The resulting constructs were introduced into flies to generate transgenic lines by using standard methods. The 5.1-kb fragment from the *tutl* RE40452 EST clone containing the full-length *tutl* cDNA was subcloned into the EcoR1 and BglII sites of the pUAST vector. Two primers 5′ ccg cgt gga tcc gct tcc aag tgt cga gga gac 3′ and 5′ tcc cca gaa ttc ggt cac ctc gca gag ata ctg 3′ were used to amplify the sequence encoding for the N-terminal three Ig domains. The PCR fragment was then subcloned into the pGEX-4T-1 expression vector for generating GST-Tutl fusion protein in bacteria. To generate the Tutl-GFP fusion construct for cell aggregation assay, the fragment encoding for the extracellular and transmembrane sequence (amino-acid 1–879) was amplified by PCR and subcloned into the UAS-GFP vector using the gateway system (Invitrogen).

Histology. Cryostat sections of pupal and adult heads and whole mount eye–brain complexes from third-instar larvae were dissected and stained as described previously (Garrity et al., 1996; Ruan et al., 1999). The anti-Tutl antibody was raised against the GST-Tutl fusion protein (see above), which contains the N-terminal three Ig-like domains shared by all putative isoforms. The antibody was affinity purified and preabsorbed using standard protocols. Antibodies were used at the following dilutions: MAb24B10 (1:100; Developmental Studies Hybridoma Bank or DSHB), monoclonal anti-βgal (1:500; DSHB), monoclonal anti-6H4 (1:10; DSHB), rabbit polyclonal anti-GFP (1:750; Invitrogen), rabbit polyclonal anti-Tutl (1:25). The secondary antibodies (Invitrogen and Jackson ImmunoResearch) were used at 1:300 dilution. Epifluorescent images were captured using a high-resolution fluorescence imaging system (Canberra Packard) and analyzed by 2D deconvolution using MetaMorph imaging software (Universal Imaging).

Cell aggregation assay. *Drosophila* S2 cells were grown in Schneider's *Drosophila* medium (Invitrogen) with 10% heat-inactivated FBS at 25°C. Cells (3×10^6/5 ml) were transfected with 1 μg of total plasmid DNA (0.5 μg of actin-GAL4 and 0.5 μg of UAS-GFP or UAS-Tutl-GFP) with Effectene (Qiagen) according to the manufacturer's instructions. At 72 h posttransfection, cells were resuspended at a concentration of 2.25×10^6/ml and agitated at 150 RPM for 1 h at room temperature. One-

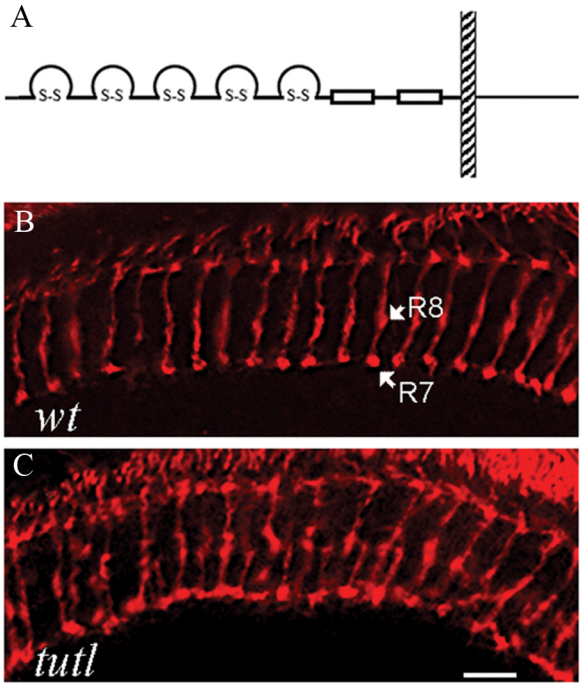

Figure 1. Mutations in *tutl* disrupted R-cell projections in the medulla. ***A***, Schematic drawing of the domain structure of the Tutl/Dasm1/IgSF9 family proteins. Open circles, Ig-like domains. Open rectangles, Fibronectin type-III repeats. ***B***, ***C***, Frozen sections of adult wild-type (***B***) and *tutl*^{01085} eye-specific mosaic (***C***) optic lobes were stained with MAb24B10 to visualize R7 and R8 axons in the medulla. Scale bars: 10 μm.

Table 1. *tutl* is required both cell-autonomously and non-cell-autonomously for R7 axonal tiling

	Wild type GFP axons	*tutl* mosaic	
		GFP axons (*tutl*)	Non-GFP (*wt*) neighbors
GMR-Flp			
Total terminals	92	80	102
Terminal fusion	9 (10%)	28 (35%)	36 (35%)
Lateral extension	11 (12%)	32 (40%)	35 (34%)
hs-Flp			
Total terminals	212	182	116
Terminal fusion	5 (2%)	33 (18%)	27 (23%)
Lateral extension	13 (6%)	63 (34%)	34 (30%)
ey$^{3.5}$-Flp			
Total terminals	43	152	63
Terminal fusion	1 (2%)	35 (23%)	9 (14%)
Lateral extension	3 (7%)	33 (22%)	22 (35%)

wt, Wild type.

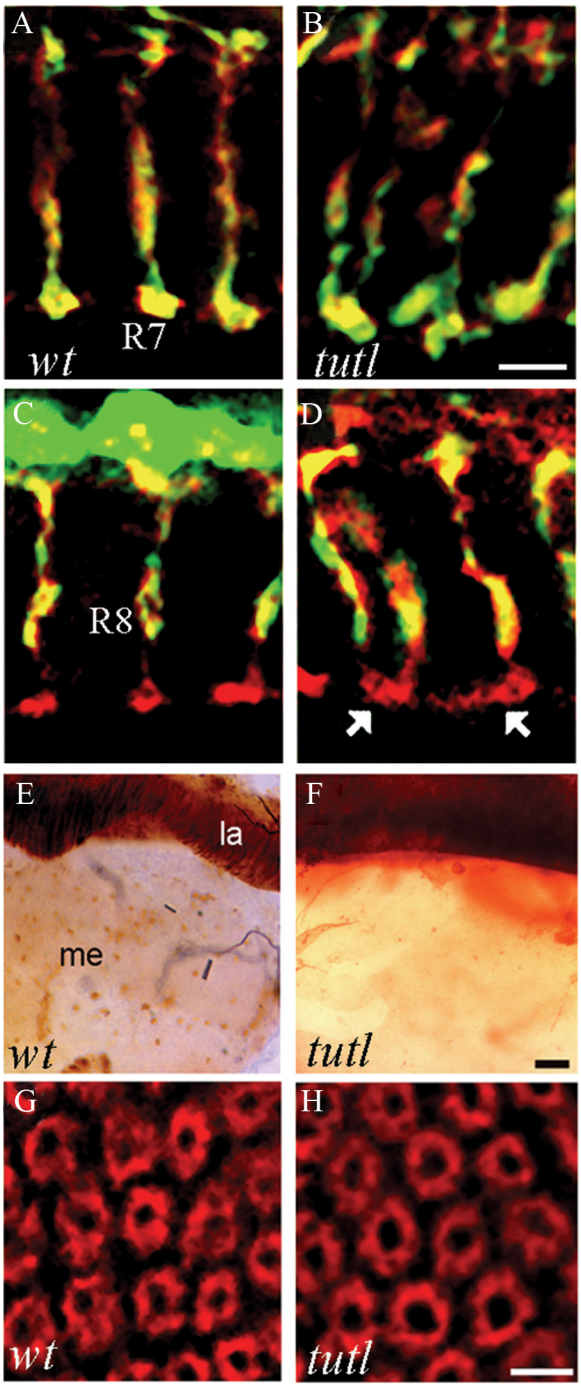

Figure 2. *tutl* mutations specifically disrupted R7 tiling. ***A–D***, Frozen sections of adult optic lobes were double-stained with MAb24B10 (red) and anti-GFP antibody (green). ***A***, ***B***, R7 axons (yellow) in wild-type (***A***) and *tutl*^{01085} eye-specific mosaic individuals (***B***) were labeled with the adult R7 marker PanGAL4-UAS-SynGFP. ***A***, In wild type, R7 axons terminate in the M6 sublayer and are restricted to regularly spaced columns in the medulla. ***B***, In *tutl*^{01085} eye-specific mosaic animals, R7 axonal terminals frequently displayed abnormal lateral extension and fusion between two neighboring terminals. ***C***, ***D***, R8 axons (green) in wild-type (***C***) and *tutl*^{01085} eye-specific mosaic individuals (***D***) were labeled with the adult R8 marker Rh5/Rh6-GAL4-UAS-synGFP. ***C***, In wild type, each R8 axon is restricted to a single column with the R7 axon from the same ommatidium and terminates in the M3 sublayer. ***D***, In *tutl*^{01085} eye-specific mosaic animals, R8 axons displayed normal columnar restriction pattern, although R7 axons within the same column still displayed defects such as abnormal lateral extension (arrow on the right) and fusion (arrow on the left). ***E***, ***F***, R1–R6 axons in whole-mount adult wild-type (***E***) and *tutl*^{01085} eye-specific mosaic (***F***) optic lobes were labeled with the R1–R6-specific marker Rh1-lacZ. Whole-mount staining allowed us to examine the entire medulla region for potential mistargeting of R1–R6 axons. In wild type (***E***), all R1–R6 axons terminate within the lamina. ***F***, No R1-R6 axon was observed in the medulla in all *tutl*^{01085} eye-specific mosaic optic lobes examined (for *ey*Flp-induced *tutl*^{01085} mutant eyes, 100%, $n > 28{,}000$ axons; for *GMR*-Flp-induced *tutl*^{01085} mutant eyes, none of positively labeled R1-R6 axons using the MARCM system in seven hemispheres showed mistargeting defects). Similar results were obtained using other *tutl* allelic combinations (i.e., *tutl*$^{01085/tutl\ 14703}$, 100%, $n > 76{,}000$ axons; *tutl*$^{14703/tutl\ 14703}$, 100%, $n > 100{,}000$ axons). ***G***, ***H***, Frozen sections of adult optic lobes were stained with presynaptic marker 6H4 to visualize lamina cartridges consisting of unlabeled processes of lamina neurons surrounded by labeled R1-R6 axons. Compared to wild type (***G***), the structure and array of lamina cartridges in *tutl*^{01085} mosaic brains (***H***) remained normal. Scale bars: ***A–D***, 5 μm; ***E***, ***F***, 20 μm; ***G***, ***H***, 5 μm.

hundred microliters of cell suspension/condition was then visualized on glass slides. To quantify the proportion of clustered GFP-expressing cells, GFP-expressing cells were counted within randomly chosen 15–20 fields at 10× magnification and noted whether these cells were present within a cell cluster of ≥5 cells. To quantify the proportion of GFP-expressing cells within each cell cluster, we randomly selected >15 cell clusters of ≥5 cells that contained at least one GFP-positive cell. We counted the number of GFP-positive cells relative to the total number of cells within each cluster.

Results

tutl mutations disrupted columnar organization of R-cell axons in the medulla

We performed phenotypic analysis to examine the effect of *tutl* mutations on R-cell connectivity. In wild type (Fig. 1*B*; Table 1), R7 and R8 axons are topographically arranged to terminate in the medulla M6 and M3 sublayers, respectively. The connections made by each R7 and R8 axons from the same ommatidium in the retina are restricted to the same column within the medulla. This regularly spaced and non-overlapping arrangement of R7 and R8 axonal terminals within medulla columns appears to involve contact-dependent repulsion. R7 and R8 axonal terminals between neighboring columns show extensive contacts at early pupal stage but then retract leading to the column-restricted connections in adults (supplemental Fig. S1, available at www.jneurosci.org as supplemental material), which is similar to that reported by Ting et al. (2005).

We performed eye-specific mitotic recombination to assess the projection of homozygous *tutl*^{01085} mutant R7 and R8 axons in an otherwise heterozygous or wild-type medulla. *tutl*^{01085} is a strong if not null allele in which a ~14 kb P-element sequence is inserted into exon 5 encoding for a portion of Ig domain 1 that disrupts the translation of the Tutl sequence downstream of Leu^{211} (Bodily et al., 2001). In *tutl* eye-specific mosaic animals in which >90% of R7 and R8 cells were homozygous for the *tutl*^{01085} mutation, we found that although R7 and R8 terminal layers were evident, the columnar organization of R7 and R8 axons in all hemispheres examined ($n > 30$) was disorganized (Fig. 1*C*). Many axonal terminals displayed abnormal lateral extension and frequently fused together, particularly at the R7 terminal layer (Fig. 1*C*). Similar phenotypic analysis was also performed using two new *tutl* alleles *tutl*^{23} and *tutl*^{GAL4} generated by us (see Materials and Methods). *tutl*^{23} is a deletion allele in which the amino-acid sequence from Glu^{133} to Ala^{754} (i.e., the five Ig-like domains and the first fibronectin-type-III repeat) of the extracellular region is deleted (see Materials and Methods). In the *tutl*^{GAL4} allele, a ~11 kb GAL4-containing P-element sequence is inserted into exon 5 of *tutl* that disrupts the translation of the sequence downstream of Leu^{211} (see Materials and Methods). Consistently, an identical phenotype was observed using the *tutl*^{23}/*tutl*^{GAL4} allelic combinations (supplemental Fig. S2, available at www.jneurosci.org as supplemental material).

tutl mutations specifically disrupted R7 tiling pattern

To specifically assess the effect of *tutl* mutations on columnar organization of R-cell axons in the medulla, we used R7- and R8-specific markers to label R7 and R8 axons in *tutl* eye-specific mosaic animals (Fig. 2*B*,*D*). We found that many R7 axonal terminals at the M6 layer (i.e., R7 recipient layer) displayed abnormal lateral extension (~46%, $n = 610$), and frequently fused between two neighboring columns (~48%, $n = 610$) (Fig. 2*B*). This defect in R7 columnar restriction is unlikely due to abnormal association (e.g., abnormal defasciculation) of R7 and R8 axons within each column due to two reasons. First, like wild type, *tutl* mutant R7 and R8 axons from the same ommatidium still associated with each other within the same column (Fig. 2*D*). Second, no obvious defect in R8 columnar restriction was observed in *tutl* mutants ($n = 455$) (Fig. 2*D*).

While severe defect in R7 columnar restriction was observed in *tutl* mutants, R-cell axonal target selection in the adult visual system appeared largely normal (Fig. 2*B*,*D*,*F*,*H*). The vast majority of R7 (Fig. 2*B*) (~99%, $n = 610$) and R8 (Fig. 2*D*) (~85%, $n = 455$) axons in *tutl* mutants terminated correctly in their medulla target layers M6 and M3, respectively. Layer-specific R1-R6 axonal target selection also remained normal in *tutl* mutants as none of *tutl* mutant R1-R6 axons examined ($n > 28{,}000$ R1-R6 axons) mis-targeted into the medulla (Fig. 2*F*). The assembly of lamina cartridges also appeared normal in all *tutl* mosaic individuals examined ($n = 6$) (Fig. 2, compare *H*, *G*). These results thus support a specific role for *tutl* in R7 tiling.

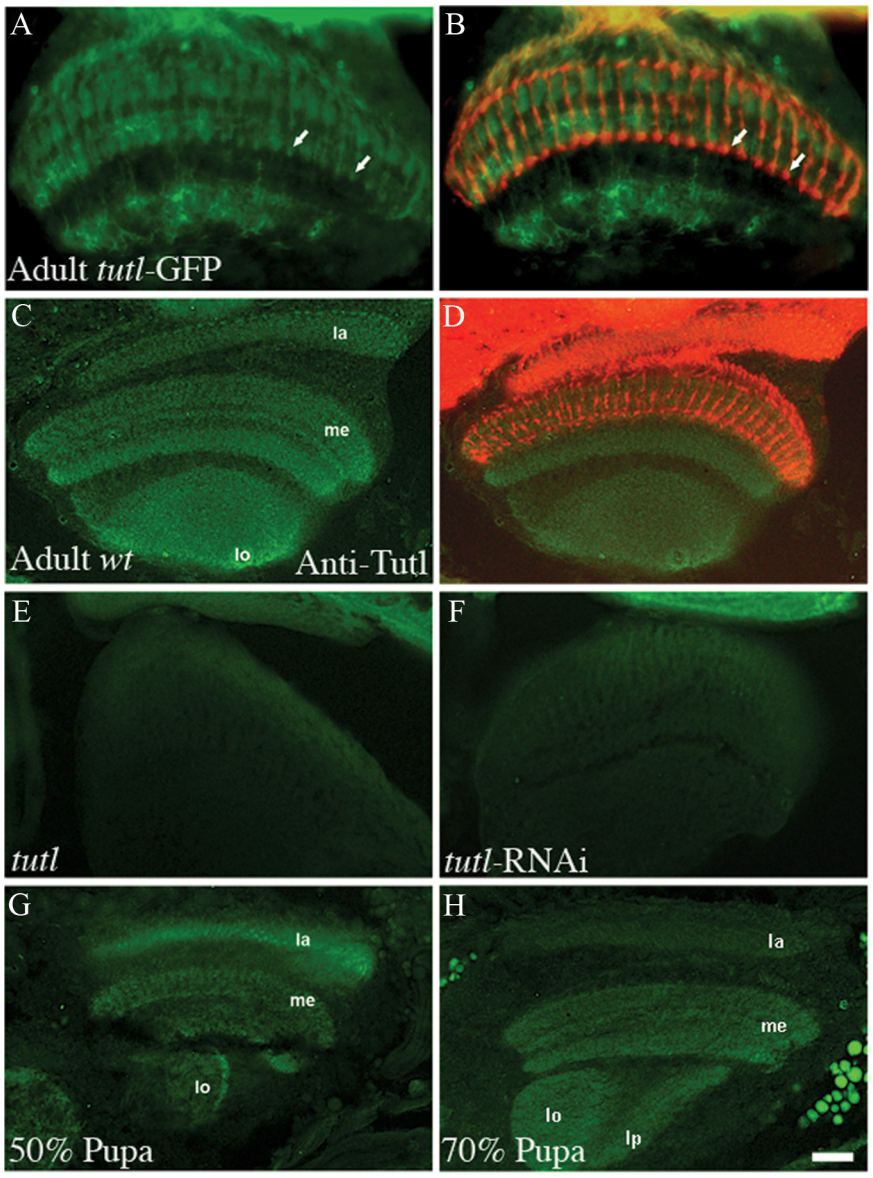

Figure 3. The expression pattern of Tutl in the visual system at developmental and adult stages. ***A***, ***B***, Adult optic lobes were dissected from wild-type flies carrying a UAS-mCD8-GFP driven by *tutl*-GAL4 and double stained with anti-GFP antibody (green) and 24B10 (red). Strong staining was detected in lamina and medulla neuropils. R7 axonal terminals were labeled (arrows). ***C***, ***D***, Frozen sections of wild-type adult optic lobes were double-stained with anti-Tutl (green) and 24B10 (red). Tutl was present in lamina, medulla and lobula neuropils at the adult stage. ***E***, Tutl staining was largely absent in $tutl^{23}/tutl^{GAL4}$ transheterozygotes. ***F***, In flies expressing a UAS-*tutl*-RNAi transgene driven by *tutl*-GAL4, Tutl immunoreactivity was significantly reduced. ***G***, ***H***, Frozen sections of wild-type 50% (***G***) and 70% pupal (***H***) optic lobes were stained with anti-Tutl antibody. la, Lamina; me, medulla; lo, lobula; lp, lobula plate. Scale bar, 20 μm.

Tutl is expressed in R7 axons and target neurons in the optic lobe

We then examined the expression pattern of Tutl in the *Drosophila* visual system. First, we generated a GAL4 transgenic line (*tutl*-GAL4) in which the GAL4 gene is inserted into exon 5 (see Materials and Methods). Since this GAL4 transgene lacks its own promoter, its expression likely reflects the expression pattern of endogenous Tutl. We examined the expression of a UAS-mCD8-GFP transgene driven by *tutl*-GAL4 at adult stages. We found that the GFP staining was detected at the R7 axonal terminals in the medulla (Fig. 3*A*,*B*, arrows), suggesting that the *tutl* gene is expressed in R7 cells. The staining was also detected in non-R7 axons in the medulla neuropil and inner optic lobe (Fig. 3*A*,*B*), suggesting that Tutl is also expressed in other types of neurons in the brain.

To determine the distribution of the Tutl protein, we performed immunostaining using an affinity-purified anti-Tutl antibody raised against a GST-Tutl fusion protein, which contains the N-terminal three Ig-like domains (see Materials and Methods). We found that Tutl staining was also detected in lamina, medulla and inner optic lobe (Fig. 3*C*,*D*). The specificity of this antibody was supported by that the staining was largely absent in *tutl* mutants (Fig. 3*E*), was significantly reduced in the optic lobe when the expression of *tutl* was knocked down by transgenic RNA interference (RNAi) under control of the *tutl*-GAL4 driver (Fig. 3*F*). Similar Tutl expression pattern was also detected at 50% (Fig. 3*G*) and 70% pupal stage (Fig. 3*H*). These results indicate that Tutl is present in the medulla neuropil during the critical period when R7 axons begin to retract and be restricted to each column.

Eye-specific expression of Tutl is sufficient for R7 tiling

To confirm that the R7 phenotype in *tutl* mutants (Fig. 1; supplemental Fig. S2, available at www.jneurosci.org as supplemental material) was indeed caused by mutations in the *tutl* locus, we tested whether knocking down the expression of *tutl* with RNA interference could cause a similar defect in R7 columnar restriction. We found that the expression of a UAS-*tutl*-RNAi transgene driven by *tutl*-GAL4 (Fig. 3) also caused a R7 tiling phenotype (Fig. 4*B*) that is indistinguishable from that in *tutl* loss-of-function mutants (Fig. 1; supplemental Fig. S2, available at www.jneurosci.org as supplemental material).

We then performed transgenic rescue experiments. A UAS-*tutl* transgene was introduced into *tutl* mutants and expressed under control of the eye-specific GMR driver. We found that eye-specific expression of this *tutl* transgene was able to rescue the R7 tiling defect in *tutl* mutants (Fig. 4*D*). This result suggests strongly that *tutl* is required in R7 axons but not in medulla target neurons for R7 tiling. Consistently, we found that R7 tiling pattern remained normal when *tutl* was selectively disrupted in the target region (100%, $n = 9$) (Fig. 4*F*).

Single-cell mosaic analysis indicates a role for Tutl in mediating interactions between adjacent R7 terminals

The R7-specific tiling phenotype, together with the expression of Tutl in R7 cells, suggest a cell-autonomous role for Tutl in specifying R7 axonal tiling. To further address this, we examined the projection of single *tutl* mutant R7 axons in an otherwise wild-type fly (see Materials and Methods). Homozygous mutant R7 cells were generated by expressing Flp recombinase under control of three different promoters (i.e., GMR, $ey^{3.5}$ and heat-shock promoters). In wild type, the vast majority of labeled single R7 axonal terminals (~90–98%) were restricted to a single column (Fig. 5*A*; Table 1). In contrast, many labeled single *tutl* mutant R7 axons displayed abnormal lateral extension (~22–40%) (Table 1). Compared to wild type, the frequency of fusion between a labeled *tutl* mutant R7 axonal terminal and its neighbors was increased by ~4–10-fold (Fig. 5*C–E*; Table 1). Among them, ~53% displayed a "U-shape" tiling phenotype, in which a mutant R7 terminal branched out from its column at the R7 recipient layer, extended laterally and fused with its neighboring R7 terminal (Fig. 5*C*,*E*). In addition, ~47% of terminal fusions displayed a "V-shape" phenotype in which a mutant R7 terminal appeared to move away from its own column and fused with its neighboring R7 terminal at the R7 recipient layer (Fig. 5*D*). These results suggest a cell-autonomous role for Tutl to control the proper spacing of R7 axonal terminals in the medulla.

The above cell-autonomous role of Tutl in R7 tiling raises two possible mechanisms for the action of Tutl. Tutl may mediate recognition between neighboring R7 terminals, which is consistent with the fact that neighboring R7 terminals contact each other extensively before the establishment of columnar restriction [supplemental Fig. S1, available at www.jneurosci.org as supplemental material (Ting et al., 2005)]. Alternatively, Tutl may mediate interactions between R7 terminals and medulla target neuronal processes that are also present between columns both before and after the establishment of R7 tiling pattern. These possibilities can be distinguished by determining whether a *tutl*-defective mutant R7 terminal affects the tiling pattern of its neighboring wild-type R7 terminals. If the Tutl-mediated R7-to-R7 recognition is required, we predict that loss of *tutl* in a mutant R7 terminal should lead to the abnormal extension of its neighboring wild-type terminals. In contrast, if the interaction between R7 terminals and medulla target processes is the key

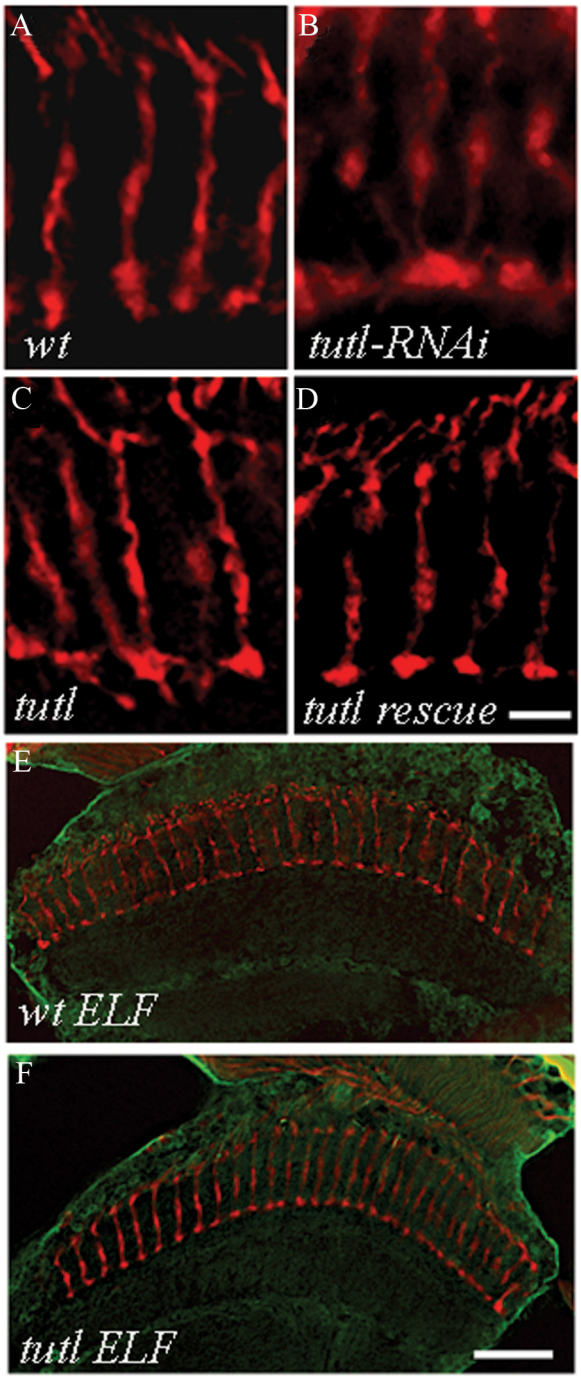

Figure 4. RNAi knockdown and transgenic rescue indicate a role for Tutl in R7 terminals to regulate R7 columnar restriction. ***A–D***, Frozen sections of adult optic lobes were stained with MAb24B10. ***A***, R7 and R8 axonal projections in wild type. ***B***, In flies expressing a UAS-*tutl*-RNAi transgene under control of *tutl*-GAL4, R7 terminals displayed abnormal lateral extension (~46%, $n = 422$) and fusion (~13%, $n = 422$). ***C***, In hypomorphic $tutl^{K14703}/tutl^{23}$ mutants, R7 terminals displayed a mild tiling phenotype (~27%, $n = 73$). ***D***, In $tutl^{K14703}/tutl^{23}$ mutants expressing a UAS-*tutl* transgene under control of the eye-specific GMR driver, the R7 terminal phenotype was rescued (~6%, $n = 317$). ***E***, ***F***, Frozen sections of adult wild-type (***E***) and $tutl^{01085}$ ELF mosaic (***F***) optic lobes were double-stained with MAb24B10 (red) and anti-GFP (green). ***E***, Wild type. ***F***, $tutl^{01085}$ ELF mosaics. Homozygous $tutl^{01085}$ mutant clones were generated in the target region but not in the eye. R7 axonal terminals in all examined $tutl^{01085}$ ELF mosaic flies ($n = 9$) were properly spaced within their respective columns. Scale bars: ***A–D***, 5 μm; ***E***, ***F***, 20 μm.

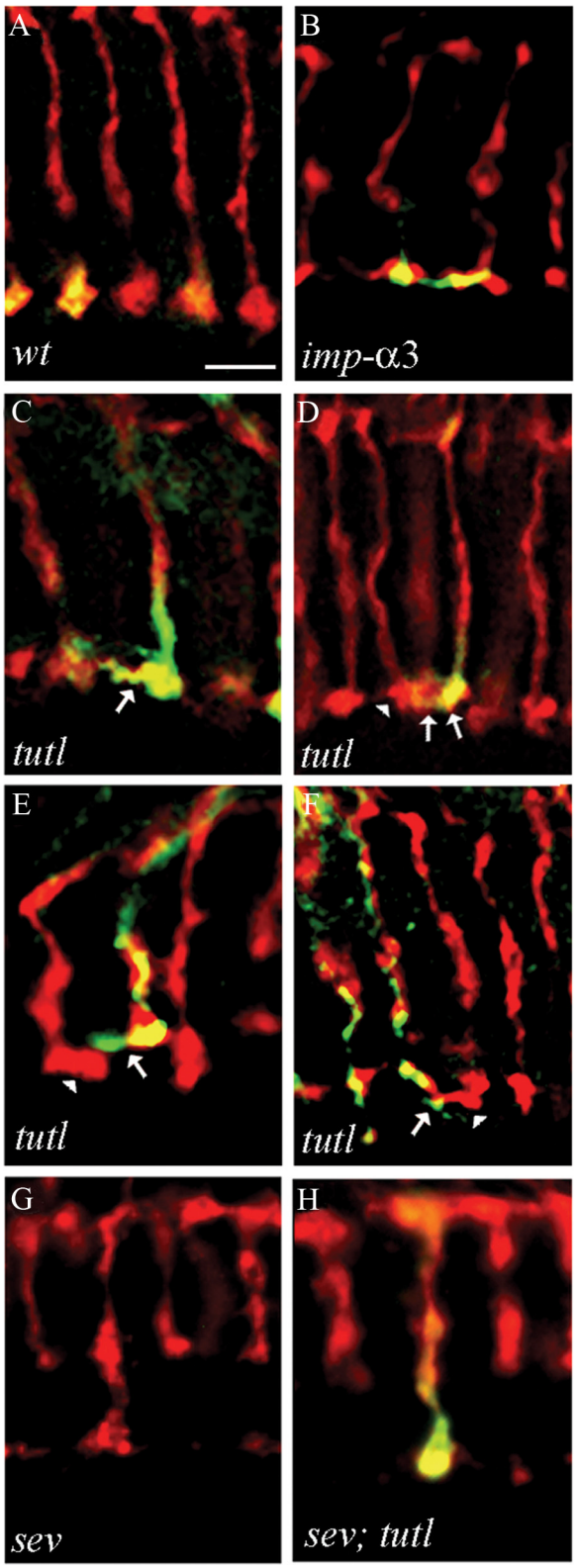

Figure 5. *tutl* is required both cell-autonomously and non-cell-autonomously for mediating R7 columnar restriction. Frozen sections of adult optic lobes were stained with MAb24B10 (red) and anti-GFP (green). ***A***, Single wild-type R7 axons were positively labeled by MARCM. Most labeled single R7 axons were restricted to their own columns without overlapping with neighboring R7 axons. ***B***, Single *imp-a3* $^{17\text{-}76}$ mutant R7 axons were generated and positively labeled by the MARCM system using GMR-Flp. The mutant R7 terminal extended a branch that invaded the neighboring wild-type column. ***C–F***, *tutl* mutant R7 axons were positively labeled by MARCM using Flp recombinase under control of heat-shock (hs) (***C***, ***D***) and GMR (***E***, ***F***) promoters. ***C***, A labeled *tutl* mutant R7 terminal (arrow) extended laterally and fused with a neighboring wild-type R7 terminal, a "U-shape" fusion phenotype. ***D***, A wild-type R7 terminal (arrowhead) moved toward its neighboring column and fused with the labeled *tutl* mutant terminal (arrow), a "V-shape" fusion phenotype. ***E***, A labeled *tutl* mutant R7 terminal (arrow) and a wild-type R7 terminal (arrowhead) extended laterally and contacted with each other at intercolumnar space. ***F***, A GFP-labeled *tutl* mutant R7 terminal (arrow) stayed within its column and was invaded by a neighboring wild-type R7 terminal (arrowhead) that selectively branched out within the R7 recipient layer. ***G***, An isolated wild-type R7 terminal stayed within its column in the absence of neighboring R7 axons. ***H***, Most of isolated *tutl* mutant R7 terminals also stayed within its own column after ablation of the neighbors. Scale bar, 5 μm.

Table 2. *tutl* interacts with the Activin pathway

Genotype	% Terminal fusion	Number of axons examined
tutl ^{01085}/+	4.1 ± 1.6	173
imp-α3 $^{17\text{-}76}$	33.1 ± 6.1	108
dActivin-RNAi	6.1 ± 3.2	218
tutl ^{01085}/+; *imp-α3* $^{17\text{-}76}$	55.7 ± 7.3[a]	114
tutl ^{01085}/+; *dActivin*-RNAi	13.9 ± 6.0[b]	283
tutl-RNAi	14.7 ± 3.0	356
tutl-RNAi; *imp-α3* $^{17\text{-}76}$	69.9 ± 6.2[a]	100
tutl-RNAi + *dActivin-RNAi*	27.8 ± 6.3[b]	305
tutl ^{01085}	18.3 ± 2.7	182
imp-α3 $^{17\text{-}76}$/+	11.8 ± 3.6	120
tutl ^{01085}; *imp-α3* $^{17\text{-}76}$/+	47.0 ± 6.0[c]	155

Homozygous *imp-α3* $^{17\text{-}76}$ and *tutl* ^{01085} mutant axons were generated and positively labeled using the MARCM system with GMR-FLP and hs-FLP, respectively.

[a]Compared to *imp-α3* $^{17\text{-}76}$ flies, the tendency of columnar invasion in *tutl* ^{01085}/+; *imp-α3* $^{17\text{-}76}$ ($p < 0.01$) and *tutl*-RNAi; *imp-α3* $^{17\text{-}76}$ ($p < 0.0001$) flies was significantly higher.

[b]The tendency of columnar invasion in *tutl* ^{01085}/+; *dActivin*-RNAi and *tutl*-RNAi + *dActivin-RNAi* flies was significantly higher than that in *dActivin*-RNAi ($p < 0.001$) and *tutl*-RNAi ($p < 0.001$), respectively.

[c]The tendency of columnar invasion in *tutl* ^{01085}; *imp-α3* $^{17\text{-}76}$/+ flies was significantly higher than that in *tutl* ^{01085} ($p < 0.0001$).

requirement for separating two R7 terminals, the prediction is that such non-cell-autonomous action of Tutl between R7 terminals should not be observed.

To determine whether *tutl* also plays a cell non-autonomous tiling role between neighboring R7 terminals, we examined the pattern of wild-type R7 axonal terminals that were neighbors of a labeled *tutl* mutant R7 axon. We found that neighboring wild-type R7 terminals also displayed a similar degree of tiling defects (Fig. 5*D–F*; Table 1). Many of them displayed abnormal lateral extension (~30–35%) (supplemental Table S1, available at www.jneurosci.org as supplemental material) and frequently extended and fused with their neighboring R7 terminal (~14–35%) (Fig. 5*E*,*F*; Table 1), indicating a cell non-autonomous tiling role for *tutl* between R7 terminals. Importantly, we found that the majority of defective wild-type R7 axons (~70%, $n = 43$) extended toward its neighboring *tutl* mutant axons (Fig. 5*E*,*F*). This result, together with that R7 tiling pattern remained normal when *tutl* was selectively disrupted in the target region (Fig. 4*F*), suggest strongly that Tutl mediates recognition between R7 terminals for the establishment of R7 tiling pattern.

Tutl functions in parallel to the activin pathway in R7 tiling

A recent report by Ting et al. (2007) shows that the Activin pathway functions cell-autonomously to control intrinsic R7 terminal growth, and acts in parallel to an unknown repulsive pathway for tiling R7 terminals. That Tutl functions in both cell-autonomous and cell non-autonomous manners to prevent the fusion of neighboring R7 terminals raises the possibility that Tutl is a key component of this repulsive pathway that acts in parallel to the Activin pathway. To test this, we examined the effect of reducing Tutl signaling on the tiling phenotype caused by loss of

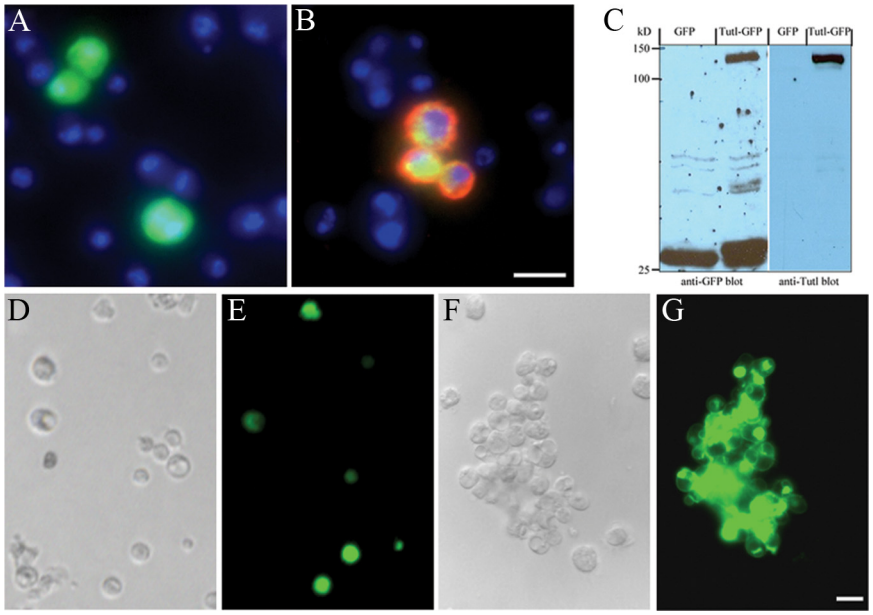

Figure 6. Tutl mediates homophilic interactions in transfected S2 cells. ***A***, ***B***, S2 cells transfected with actin-GAL4 and either UAS-GFP (***A***) or UAS-Tutl-GFP (***B***) were stained with anti-GFP (green) and anti-Tutl (red) antibodies under non-permeabilized conditions, and then counter-stained with Hoechst (blue). Anti-Tutl recognizes the extracellular region of Tutl. ***A***, GFP control. ***B***, Tutl-GFP was targeted properly onto the plasma membrane. ***C***, Western blot analysis using anti-GFP (left) or anti-Tutl (right) detected a major band at ~124 kDa in Tutl-GFP, but not GFP control transfected cell lysates, which is consistent with the predicted size of Tutl-GFP fusion protein. ***D–G***, Transfected *Drosophila* S2 cells were examined in a cell aggregation assay. ***D***, ***E***, Cells transfected with GFP control remained largely as single cells following the aggregation assay. ***F***, ***G***, Tutl-GFP-transfected cells selectively aggregated with each other but not with Tutl-negative cells. Compared to GFP control (6.7 ± 0.7%), the tendency of a Tutl-GFP-expressing cell (20.9 ± 2.4%) to be recruited into cell clusters (≥5 cells) was increased by three-fold. Compared to GFP control (19.6 ± 1.9%), each Tutl-GFP-transfected cell clusters ($n > 15$ cell clusters) included predominantly Tutl-positive cells (82.2 ± 3.7%). $p < 0.001$. Scale bar, 10 μm.

importin-α3 (*imp-α3*) (Fig. 5*B*), which is required for targeting dSmad2 into the nucleus for tiling R7 terminals (Ting et al., 2007). Indeed, we found that reducing the level of Tutl significantly enhanced the tendency of the *imp-α3* mutant axons to invade neighboring columns (Table 2). Conversely, reducing the level of *imp-α3* also significantly enhanced the frequency of the *tutl* tiling phenotype (Table 2). Consistently, reducing the level of *tutl* significantly enhanced the tiling phenotype induced by knocking down the expression of *dActivin* (Table 2). These results are thus consistent with that the Tutl pathway acts in parallel to Activin signaling.

Since *imp-α3* and *tutl* phenotypic analysis relied on genetic mosaic analysis due to larval lethality, mutant clones generated by mitotic recombination may not be completely null due to perdurance. Thus, while that above genetic interaction data are consistent with that the Turtle pathway acts in parallel to the Activin pathway, it does not exclude the possibility that Tutl and Activin functions in the same pathway. To further address this, we performed genetic ablation experiments to determine the effect of removing neighboring R7 axons on the pattern of a *tutl* mutant R7 axon. Previous studies by Ting et al. (2007) showed that removing neighboring R7 terminals greatly increased the frequency of the *imp-α3* tiling phenotype from 23.0% for mutant R7 axons surrounded by neighboring R7 terminals to 84.3% ($n = 32$) for isolated mutant R7 axons. This result suggested the presence of a repulsive pathway that acts in parallel to the Activin pathway. We reasoned that if Tutl and Activin function in the same pathway that controls terminal growth but not repulsion, the prediction is that removing neighboring R7 terminals would also increase the frequency of the *tutl* phenotype. In contrast, no such enhancement should be observed with ablation if Tutl mediates repulsion. Our results showed that in the absence of neighboring R7 terminals, the tendency of a *tutl* mutant axon to invade neighboring column was decreased from ~33% ($n = 81$) for surrounded R7 terminals to ~15% ($n = 45$) for isolated R7 terminals (Fig. 5*H*). This result, together with that Tutl is required both cell autonomously and cell non-autonomously to prevent R7 terminal fusion (Fig. 5*E*,*F*), support that Tutl functions in parallel to the Activin pathway to regulate R7 tiling.

Tutl mediates homophilic cell–cell interactions in transfected S2 cells

That Tutl functions both cell autonomously and cell non-autonomously in R7 tiling raises the possibility that Tutl mediates homophilic interactions. To address this, we performed cell aggregation experiments using transfected S2 cells. S2 cells have low adhesivity and are widely used to determine the binding property of cell adhesion molecules (Shinza-Kameda et al., 2006). S2 cells were transiently transfected with GFP control and Tutl-GFP fusion constructs. Cell aggregation assay was performed by gently shaking transfected cells for 1 h. We found that Tutl expression significantly increased the probability of transfected cells to be recruited into cell clusters. While >20% of Tutl transfected cells were found in cell clusters containing five or more cells (Fig. 6*G*), only ~5% of GFP control cells were recruited into cell clusters (Fig. 6*E*). We also observed that Tutl-expressing cells selectively aggregated with each other as none or only a very few Tutl-negative cells were found in each cell clusters (Fig. 6*G*). These results indicate that Tutl mediates cell–cell interactions in a homophilic manner.

Discussion

Our results indicate an essential and specific role for Tutl in the establishment of column-specific R7 connections in the *Drosophila* visual system. Loss of Tutl causes a failure of R7 terminals to separate from each other leading to R7 tiling defects. Tutl is required in R7 axons but not in medulla target neurons for the restriction of R7 connections to single columns. Genetic interaction and ablation analyses indicate that Tutl functions in parallel to the Activin pathway to control R7 tiling. That Tutl functions in both cell-autonomous and cell-non-autonomous manners to prevent the fusion of adjacent R7 terminals, together with that Tutl mediates homophilic cell–cell interactions in transfected S2 cells, suggest a model in which the Tutl-mediated terminal–terminal recognition functions together with the Activin-mediated intrinsic growth control to restrict the connection of each R7 terminal to a single column.

Restriction of R7 connections to single columns requires both repulsion between R7 terminals and the control of intrinsic R7 terminal growth (Ashley and Katz, 1994; Ting et al., 2007). A recent study by Ting et al. (2007) provides convincing evidence that the restriction of intrinsic R7 terminal growth is mediated by the Activin pathway, which functions together with an unknown

parallel mechanism that mediates mutual repulsion between adjacent R7 terminals. The requirement of mutual repulsion in R7 columnar restriction is not surprising. R7 terminals show extensive contacts with each other before segregation into separate columns. Given the expression of a number of cell adhesion molecules such as N-Cadherin and Chaoptin on R7 terminals throughout development (Van Vactor et al., 1988; Lee et al., 2001), it seems clear that a repulsive force or an anti-adhesion mechanism is necessary to overcome the adhesion and thus facilitate the segregation of adjacent R7 terminals. Mutual repulsion has been suggested to be required for columnar restriction of L1 neurons in the *Drosophila* visual system, which is mediated by Dscam2 (Millard et al., 2007). Up to now, Dscam2 and its mouse homolog Dscam are only known cell surface transmembrane proteins to be implicated in mediating mutual repulsion for axonal/dendrite tiling (Millard et al., 2007; Fuerst et al., 2008). In addition, Dscam and the receptor tyrosine phosphatase HmLAR2 have been shown to be involved in mediating self-avoidance, a phenomenon referring to the avoidance of sister neurites projected from a single neuron, in sensory neurons in *Drosophila* (Hughes et al., 2007; Matthews et al., 2007; Soba et al., 2007) and the comb cell in Leech (Gershon et al., 1998), respectively.

That Dscam2 is not required for R7 tiling (Millard et al., 2007) indicates the involvement of other cell surface proteins in mediating the repulsive interaction between adjacent R7 terminals. Our results suggest that Tutl is an essential component of this repulsive pathway that functions in parallel to the Activin pathway to restrict the connections of R7 terminals to single columns. First, in *tutl* mutants, fusion between neighboring R7 terminals were frequently observed at the R7 recipient layer in the medulla, consistent with a role for Tutl to antagonize the adhesion between adjacent R7 terminals. Second, unlike that the Activin pathway functions cell-autonomously in restricting intrinsic R7 terminal growth, Tutl is required both cell-autonomously and cell-non-autonomously for R7 tiling. In *tutl* mosaics, loss of *tutl* in a single R7 terminal could lead to the invasion of a wild-type column by a neighboring mutant R7 terminal, the invasion of a mutant column by a neighboring wild-type R7 terminal, or the fusion of adjacent mutant and wild-type R7 terminals at intercolumnar space. Third, reducing the level of *tutl* or *imp-α3* significantly increased the frequency of tiling defect in *imp-α3* or *tutl* mutants, respectively. And fourth, ablation of neighboring R7 terminals decreased the frequency of *tutl* tiling phenotype, which is in marked contrast to the enhancement of Activin tiling phenotype with genetic ablation of neighboring R7 terminals. Those results are consistent with that Tutl mediates the recognition between neighboring R7 terminals to restrict their connections to a single column.

There are several possible mechanisms for the action of Tutl in preventing fusion between neighboring R7 terminals. For instance, like the action of Semaphoring-1a and Plexin-A in motor axon de-fasciculation (Winberg et al., 1998; Yu et al., 1998), Tutl may directly trigger a repulsive response between neighboring R7 terminals, thus forcing the separation of R7 terminals. Alternatively, Tutl may act to interfere with the function of certain cell adhesion molecules, thus downregulating the attraction between neighboring R7 terminals. Our current data does not allow us to distinguish among these possibilities.

Our results reveal for the first time the *in vivo* cellular action of the novel and conserved Tutl/Dasm1/IgSF9 family in the developing nervous system. While *tutl* was previously reported to be required for larval coordinated movement and adult flight behaviors (Bodily et al., 2001), neural basis of those behavioral phenotypes remains unclear. That *tutl* mutants do not show detectable morphological defects in the ventral nerve cod and neuromuscular junctions led to the speculation that Tutl may be required for the connectivity of a very small subset of neurons (Bodily et al., 2001). Consistent with this view, our results show that *tutl* functions on a fine scale to restrict the connections of R7 terminals to single columns, but it is not required for the targeting of R7 axons from the retina into the R7 recipient layer nor involved in R8 columnar restriction in the medulla. We propose that Tutl functions to prevent fusion between adjacent R7 terminals by mediating mutual repulsion or interfering with adhesion. Similar Tutl-mediated cell surface recognition may also be used by other neurons to refine neuronal circuits necessary for controlling larval and adult coordinated movements.

The *in vivo* function of Dasm1 and IgSF9, the mouse and human homologs of Tutl, remains unknown. Previous *in vitro* studies show that Dasm1-RNAi knockdown impaired dendrite growth and synaptic maturation in cultured hippocampal neurons (Shi et al., 2004a,b). However, a recent study shows that Dasm1 null mutants displayed normal dendritic arborization pattern *in vivo* and *in vitro* (Mishra et al., 2008). One possible explanation for normal dendritic growth in Dasm1 null mice is that Dasm1 may be functionally redundant with its close homolog IgSF9b in regulating dendritic patterning in the developing hippocampus. Alternatively or additionally, Dasm1 may function in other brain regions to regulate different developmental events. Thus, it will be of interest to determine whether Dasm1 and IgSF9 also play a similar role in specifying columnar restriction and/or axonal/dendritic tiling in the mammalian nervous system.

References

Ashley JA, Katz FN (1994) Competition and position-dependent targeting in the development of the *Drosophila* R7 visual projections. Development 120:1537–1547.

Bodily KD, Morrison CM, Renden RB, Broadie K (2001) A novel member of the Ig superfamily, turtle, is a CNS-specific protein required for coordinated motor control. J Neurosci 21:3113–3125.

Chotard C, Leung W, Salecker I (2005) glial cells missing and gcm2 cell autonomously regulate both glial and neuronal development in the visual system of *Drosophila*. Neuron 48:237–251.

Clandinin TR, Zipursky SL (2002) Making connections in the fly visual system. Neuron 35:827–841.

Dietzl G, Chen D, Schnorrer F, Su KC, Barinova Y, Fellner M, Gasser B, Kinsey K, Oppel S, Scheiblauer S, Couto A, Marra V, Keleman K, Dickson BJ (2007) A genome-wide transgenic RNAi library for conditional gene inactivation in *Drosophila*. Nature 448:151–156.

Doudney K, Murdoch JN, Braybrook C, Paternotte C, Bentley L, Copp AJ, Stanier P (2002) Cloning and characterization of Igsf9 in mouse and human: a new member of the immunoglobulin superfamily expressed in the developing nervous system. Genomics 79:663–670.

Fuerst PG, Koizumi A, Masland RH, Burgess RW (2008) Neurite arborization and mosaic spacing in the mouse retina require DSCAM. Nature 451:470–474.

Garrity PA, Rao Y, Salecker I, McGlade J, Pawson T, Zipursky SL (1996) *Drosophila* photoreceptor axon guidance and targeting requires the dreadlocks SH2/SH3 adapter protein. Cell 85:639–650.

Gershon TR, Baker MW, Nitabach M, Macagno ER (1998) The leech receptor protein tyrosine phosphatase HmLAR2 is concentrated in growth cones and is involved in process outgrowth. Development 125:1183–1190.

Grueber WB, Ye B, Moore AW, Jan LY, Jan YN (2003) Dendrites of distinct classes of *Drosophila* sensory neurons show different capacities for homotypic repulsion. Curr Biol 13:618–626.

Hughes ME, Bortnick R, Tsubouchi A, Bäumer P, Kondo M, Uemura T, Schmucker D (2007) Homophilic Dscam interactions control complex dendrite morphogenesis. Neuron 54:417–427.

Kramer AP, Kuwada JY (1983) Formation of the receptive fields of leech mechanosensory neurons during embryonic development. J Neurosci 3:2474–2486.

Lee CH, Herman T, Clandinin TR, Lee R, Zipursky SL (2001) N-cadherin regulates target specificity in the *Drosophila* visual system. Neuron 30:437–450.

Lee T, Luo L (1999) Mosaic analysis with a repressible cell marker for studies of gene function in neuronal morphogenesis. Neuron 22:451–461.

Lin B, Wang SW, Masland RH (2004) Retinal ganglion cell type, size, and spacing can be specified independent of homotypic dendritic contacts. Neuron 43:475–485.

Matthews BJ, Kim ME, Flanagan JJ, Hattori D, Clemens JC, Zipursky SL, Grueber WB (2007) Dendrite self-avoidance is controlled by Dscam. Cell 129:593–604.

Meinertzhagen IA, Hanson TE (1993) The development of the optic lobe. In: The development of *Drosophila melanogaster* (Bates M, Arias AM, eds), pp 1363–1492. Cold Spring Harbor, NY: Cold Spring Harbor UP.

Millard SS, Flanagan JJ, Pappu KS, Wu W, Zipursky SL (2007) Dscam2 mediates axonal tiling in the *Drosophila* visual system. Nature 447: 720–724.

Mishra A, Knerr B, Paixão S, Kramer ER, Klein R (2008) The protein dendrite arborization and synapse maturation 1 (Dasm-1) is dispensable for dendrite arborization. Mol Cell Biol 28:2782–2791.

Mountcastle VB (1997) The columnar organization of the neocortex. Brain 120:701–722.

Newsome TP, Asling B, Dickson BJ (2000) Analysis of *Drosophila* photoreceptor axon guidance in eye-specific mosaics. Development 127:851–860.

Parks AL, Cook KR, Belvin M, Dompe NA, Fawcett R, Huppert K, Tan LR, Winter CG, Bogart KP, Deal JE, Deal-Herr ME, Grant D, Marcinko M, Miyazaki WY, Robertson S, Shaw KJ, Tabios M, Vysotskaia V, Zhao L, Andrade RS, et al. (2004) Systematic generation of high-resolution deletion coverage of the *Drosophila melanogaster* genome. Nat Genet 36:288–292.

Perry VH, Linden R (1982) Evidence for dendritic competition in the developing retina. Nature 297:683–685.

Ruan W, Pang P, Rao Y (1999) The SH2/SH3 adaptor protein dock interacts with the Ste20-like kinase misshapen in controlling growth cone motility. Neuron 24:595–605.

Sepp KJ, Auld VJ (1999) Conversion of lacZ enhancer trap lines to GAL4 lines using targeted transposition in *Drosophila melanogaster*. Genetics 151:1093–1101.

Shi SH, Cheng T, Jan LY, Jan YN (2004a) The immunoglobulin family member dendrite arborization and synapse maturation 1 (Dasm1) controls excitatory synapse maturation. Proc Natl Acad Sci U S A 101: 13346–13351.

Shi SH, Cox DN, Wang D, Jan LY, Jan YN (2004b) Control of dendrite arborization by an Ig family member, dendrite arborization and synapse maturation 1 (Dasm1). Proc Natl Acad Sci U S A 101:13341–13345.

Shinza-Kameda M, Takasu E, Sakurai K, Hayashi S, Nose A (2006) Regulation of layer-specific targeting by reciprocal expression of a cell adhesion molecule, capricious. Neuron 49:205–213.

Soba P, Zhu S, Emoto K, Younger S, Yang SJ, Yu HH, Lee T, Jan LY, Jan YN (2007) *Drosophila* sensory neurons require Dscam for dendritic self-avoidance and proper dendritic field organization. Neuron 54:403–416.

Ting CY, Yonekura S, Chung P, Hsu SN, Robertson HM, Chiba A, Lee CH (2005) *Drosophila* N-cadherin functions in the first stage of the two-stage layer-selection process of R7 photoreceptor afferents. Development 132:953–963.

Ting CY, Herman T, Yonekura S, Gao S, Wang J, Serpe M, O'Connor MB, Zipursky SL, Lee CH (2007) Tiling of r7 axons in the *Drosophila* visual system is mediated both by transduction of an activin signal to the nucleus and by mutual repulsion. Neuron 56:793–806.

Van Vactor D Jr, Krantz DE, Reinke R, Zipursky SL (1988) Analysis of mutants in chaoptin, a photoreceptor cell-specific glycoprotein in *Drosophila*, reveals its role in cellular morphogenesis. Cell 52:281–290.

Wässle H, Peichl L, Boycott BB (1981) Dendritic territories of cat retinal ganglion cells. Nature 292:344–345.

Winberg ML, Noordermeer JN, Tamagnone L, Comoglio PM, Spriggs MK, Tessier-Lavigne M, Goodman CS (1998) Plexin A is a neuronal semaphorin receptor that controls axon guidance. Cell 95:903–916.

Yu HH, Araj HH, Ralls SA, Kolodkin AL (1998) The transmembrane Semaphorin Sema I is required in *Drosophila* for embryonic motor and CNS axon guidance. Neuron 20:207–220.